NANO LETTERS

2004
Vol. 4, No. 10
2051−2055

Single-Crystal Calcium Hexaboride Nanowires: Synthesis and Characterization

Terry T. Xu,[†] Jian-Guo Zheng,[‡] Alan W. Nicholls,[§] Sasha Stankovich,[†] Richard D. Piner,[†] and Rodney S. Ruoff*,[†]

Department of Mechanical Engineering, Northwestern University, Evanston, Illinois 60208, NUANCE Center, Northwestern University, Evanston, Illinois 60208, and Research Resource Center, University of Illinois at Chicago, Chicago, Illinois 60612

Received August 17, 2004

ABSTRACT

Catalyst-assisted growth of single-crystal calcium hexaboride (CaB_6) nanowires was achieved by pyrolysis of diborane (B_2H_6) over calcium oxide (CaO) powders at 860–900 °C and ~155 mTorr in a quartz tube furnace. TEM electron diffraction and Raman spectroscopy indicate that the nanowires are single-crystal CaB_6 and have a preferred [001] growth direction. Analysis of TEM/EDX/EELS data proves the nanowires consist of CaB_6 cores and thin (1–2 nm) amorphous oxide shell material. The CaB_6 nanowires have diameters of ~15–40 nm, and lengths of ~1–10 μm.

Calcium hexaboride (CaB_6), one of the divalent alkaline-earth cubic hexaborides, has low density (2.45 g/cm^3), high melting point (2235 °C), high hardness (Knoop: 2600 kg/mm^2), high Young's modulus (379 GPa), and high chemical stability.[1,2] CaB_6 has found application as a high-temperature material, is used for surface protection, and as a wear resistant material.[1,2] CaB_6 is also a promising candidate for n-type thermoelectric (TE) materials, because its power factor has been reported to be larger than or comparable to that of common TE materials (i.e., Bi_2Te_3, PbTe, $Si_{1-x}Ge_x$).[3,4] Recently, the discovery of weak ferromagnetism in La-doped CaB_6,[5] undoped CaB_6[6], and CaB_2C_2[7] has attracted much attention because of their respective high Curie temperatures (>600 K) but with the absence of a 3d or 4f element in each compound. The mechanisms for the observed ferromagnetism in these compounds have been explored with both experiment and theory.[8,9] There is no agreement, however, as to whether the ferromagnetism is extrinsic or intrinsic,[10−12] and also whether CaB_6 is semimetallic[13−15] or semiconducting.[16,17]

CaB_6 bulk crystals have been prepared at elevated temperature (>1500 °C) by hot-press sintering,[18] the floating zone method,[19] and the aluminum flux method.[20] CaB_6 powders have been prepared by direct combination of boron (B) with calcium (Ca) at 1000 °C in a sealed tantalum crucible,[21] by carbothermal reduction of calcium carbonate ($CaCO_3$) and boron carbide (B_4C) at 1400 °C and 10^{-2} Pa,[22] by reduction of calcium oxide (CaO) with B at 1200−1800 °C in vacuum,[3] and by reaction of calcium chloride ($CaCl_2$) with sodium borohydride ($NaBH_4$) at 500 °C in an autoclave for 8 h.[23] The finest crystalline CaB_6 powders synthesized so far have an average size of 180 nm.[23]

Stimulated by the theoretical prediction of metallic single-walled boron[24] and aluminum boride (AlB_2) nanotubes,[25] we and others are motivated to attempt synthesis of boron and boron-rich one-dimensional (1D) nanomaterials. For example, boron nanowires,[26−30] nanobelts,[31] and nanoribbons[32] have been synthesized by magnetron sputtering,[26] laser ablation,[27,30,31] and chemical vapor deposition (CVD).[28,29,32] Chromium boride (CrB) nanorods were synthesized by reaction of chromium trichloride ($CrCl_3$) and B powders in molten sodium at 650 °C in an autoclave.[33] Magnesium diboride (MgB_2) nanowires were synthesized by exposing amorphous B nanowires to Mg vapor at 800−900 °C,[34] or by direct pyrolysis of MgB_2 nanoparticles at 900 °C.[35]

In this letter, we report the catalyst-assisted growth of CaB_6 nanowires by pyrolysis of diborane (B_2H_6) over CaO powders at 860−900 °C and ~155 mTorr. Nickel (Ni) is found to be an effective catalytic material. To our knowledge, this is the first report on synthesis of 1D CaB_6 nanostructures, and it was achieved at relatively low temperature. Such CaB_6 nanowires have potential use in nanocomposites where they may impart stiffness, toughness, and strength. They also show promise for use in nanoelectronics, including in high temperature environments, or when low weight is imperative

* Corresponding author. Telephone: (847) 467-6596. Fax: (847) 491-3915. E-mail: r-ruoff@northwestern.edu.
[†] Department of Mechanical Engineering, Northwestern University.
[‡] NUANCE Center, Northwestern University.
[§] Research Resource Center, University of Illinois at Chicago.

10.1021/nl0486620 CCC: $27.50
Published on Web 09/16/2004

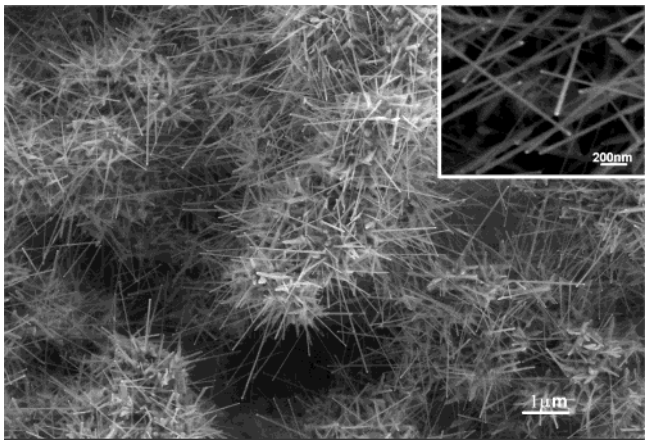

Figure 1. SEM micrograph of as-synthesized CaB_6 nanowires. The inset shows an enlarged view of the nanowires. Catalyst particles (bright white) can be observed on the nanowire tips.

(such as for aerospace needs). Moreover, the as-synthesized nanowires can be used to investigate the currently controversial electrical and magnetic properties of CaB_6, but on nanoscale samples.

Our experiments were carried out in a home-built low-pressure CVD (LPCVD) system described elsewhere.[32] Silicon (Si) substrates with one-micron thick thermally grown SiO_2 (University Wafer; 1×2 cm^2) were used for the experiments. The substrates were ultrasonically cleaned using acetone and ethanol (Crest ultrasonic cleaner; 5 min), followed by oxygen plasma cleaning (Plasma-862, Kurt J. Lesker; 3 min). CaO powders (Alfa Aesar; 99.998% purity) were randomly deposited on the Si substrates. A thin Ni layer (1−2 nm) was then evaporated on the CaO-coated Si substrate by an e-beam evaporator (BOC Edward; 360 series). The substrates were loaded in a quartz boat and placed in a 1-in. diameter quartz tube reaction chamber. The chamber temperature was ramped up to 900 °C (center position temperature) in 60 min with 5 sccm (standard cubic centimeters per minute) continuous flow of argon (BOC gases; 99.999% purity). A gas mixture of diborane (Voltaix; 5% UHP diborane in research grade argon; flow rate: 15 sccm) and argon (flow rate: 5 sccm) was then introduced into the chamber for 20 min. The reaction pressure for each run was ∼155 mTorr (for any particular run, the pressure was measured to 3 significant figures). After reaction, the chamber was cooled to room temperature in ∼5 h under 5 sccm argon flow. The substrates were taken out and characterized by scanning electron microscopy (SEM; LEO 1525 FE-SEM), transmission electron microscopy (TEM) including electron diffraction (Hitachi H-8100), high-resolution TEM (HR-TEM; Hitachi HF-2000), electron energy loss spectroscopy (EELS; Hitachi HF-2000, JEOL JEM 2010F), energy-dispersive X-ray spectroscopy (EDX; Hitachi HF-2000, JEOL JEM 2010F), and Raman spectroscopy (Renishaw 2000; 514.5 nm argon ion laser excitation).

Wire-like nanostructures were synthesized on the substrates placed in the ∼3 cm long 860−900 °C temperature zone of the reaction chamber. Though various morphologies were observed at different positions along the temperature gradient (discussed in detail below), the nanowires are

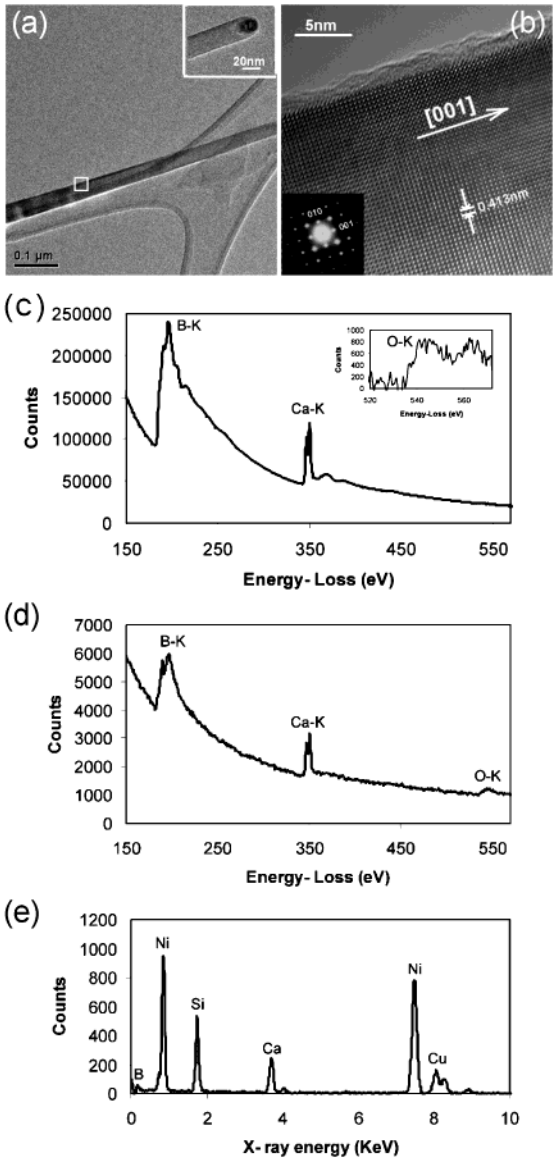

Figure 2. (a) TEM micrographs of a portion of one nanowire. The inset shows a catalytic particle on the tip of the nanowire. (b) HR-TEM image of the section enclosed by the white square in Figure 2a, showing a crystallized structure and preferential growth along the [001] direction. An amorphous layer (1−2 nm thick) is clearly identified as the outer shell. The inset is a representative diffraction pattern recorded along the [$\bar{1}$00] zone axis. (c) An EELS spectrum recorded at the center of one nanowire shows the high-intensity B and Ca K-shell ionization edges at ∼188 and 346 eV, respectively. The inset shows the weak-intensity O K-shell ionization edge at ∼532 eV. (d) An EELS spectrum recorded from the edge of one nanowire, showing B, Ca, and O K-shell ionization edges. Note: The O K-shell ionization edge is more obvious in this spectrum. (e) An EDX spectrum recorded from the catalytic particle, showing the presence of Ca, B, Ni, and Si.

roughly ∼15−40 nm in diameter, and ∼1−10 μm in length. Catalyst particles could be observed on the tips of most of the nanowires. Figure 1 is a low-magnification SEM image of the as-synthesized nanowires. A high magnification image of these nanowires (Figure 1 inset) shows the catalyst particles on the tips.

Figure 2a is a low-magnification TEM micrograph, showing a portion of a typical nanowire. The inset shows the

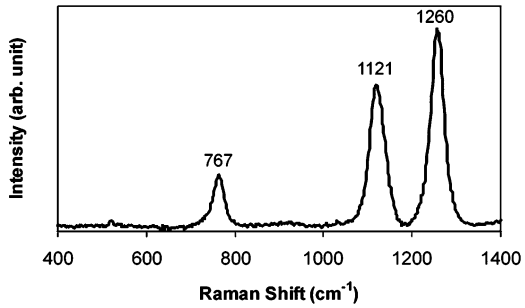

Figure 3. Raman spectrum of as-synthesized nanowires. The three peaks at ~767, 1121, and 1260 cm^{-1} are assigned to the CaB_6 Raman active modes A_{1g}, E_g, and T_{2g}, respectively.

catalyst particle on the tip of the nanowire. Figure 2b is a HR-TEM image of the section enclosed by the white square in Figure 2a. The nanowire is well crystallized and covered by a 1−2 nm thick amorphous layer. Electron diffraction was done on tens of nanowires to determine their structures, and the same diffraction patterns were always obtained. The calculated lattice constant is $a = 0.413 \pm 0.005$ nm, which is close to that of cubic CaB_6 from the JCPDS database (#65-1830, $a = 0.4145$ nm; #31−0254, $a = 0.4154$ nm). The inset in Figure 2b is a diffraction pattern recorded in the $[\bar{1}00]$ axis. Based on HR-TEM and electron diffraction analysis, the growth direction of as-synthesized nanowires was determined to be the [001] direction. EELS line scans (STEM mode; probe size 0.2 nm) were performed to study the element distribution in the nanowires. Figures 2c and 2d are two typical EELS spectra recorded from the center and the edge of one nanowire, respectively. Both spectra show the characteristic B, Ca, and O K-shell ionization edges at ~188, ~346, and ~532 eV, respectively. However, the O K-shell ionization edge recorded from the amorphous shell of the nanowire (Figure 2d) is more obvious than that from the center of the nanowire (Figure 2c), indicating an oxide layer was formed at the periphery of the nanowire. Moreover, the change in the fine structure of the B K-shell ionization edge between the center and edge of the wire implies a change in bonding between the boron and other elements present. EDX (STEM mode; 1 nm probe size) was used to study the chemical composition of the catalyst. Figure 2e is a representative EDX spectrum recorded from one catalyst particle, from which Ca, B, Ni, and Si were identified (the Cu signal comes from the supporting Cu grid and is not a component of the nanowires). From the TEM/EELS/EDX analysis, the as-synthesized nanowires have a single-crystal CaB_6 core and a thin amorphous layer surrounding the core containing Ca, B, and O. The catalyst material consists of Ca, B, Ni, and Si.

Figure 3 shows the Raman spectrum of the as-synthesized nanowires acquired at room temperature in ambient. The peaks at 767, 1121, and 1260 cm^{-1} match the Raman active modes A_{1g}, E_g, and T_{2g}, respectively, of CaB_6.[36,37] Table 1 summarizes peak positions of CaB_6 in different form. The shift and broadening of Raman peaks observed in this work may be due to the size-confinement effect, internal lattice strain induced by defects and impurities, and local intense heating.[38−40]

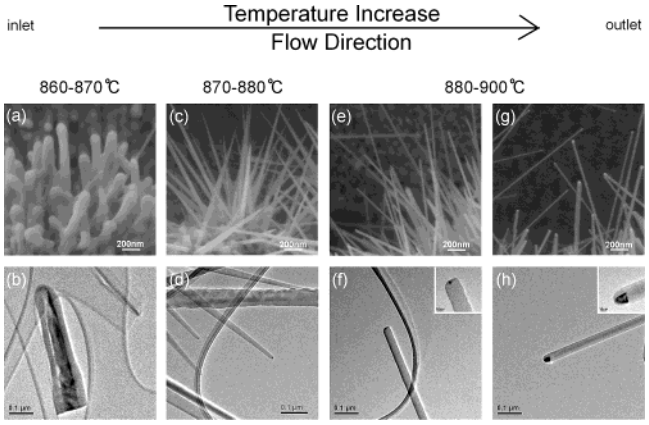

Figure 4. Electron micrographs of CaB_6 nanowires differing in morphology observed along the 860−900 °C, ~3 cm long temperature gradient in our reaction chamber (see text for details).

Table 1. Summary of Raman Peak Positions of CaB_6

materials	Peak Position (cm^{-1})		
	A_{1g}	E_g	T_{2g}
calculated values[41]	1314	1181	728
CaB_6 coarse powders[37]	1270	1125	775
bulk single-crystal CaB_6[36]	1290	1150	780
single-crystal CaB_6 ultrafine powders [23]	1247	1122	754
single-crystal CaB_6 nanowires[a]	1260	1121	767

[a] Measured in this work.

As mentioned above, nanowires with different morphologies were observed at positions along the 860−900 °C temperature gradient (~3 cm long) in the reaction chamber. Figures 4a−h are electron micrographs of four different morphologies. Figures 4a,c,e,g are SEM micrographs, and Figures 4b,d f,h are the corresponding TEM images. At lower temperature (~860−870 °C), short and thick nanowires were observed as shown in Figures 4a and 4b. TEM combined with EDX line scan analyses revealed the nanowires to have a CaB_6 core and amorphous shell containing primarily B with small amounts of Si and O. In the higher temperature zone (870−880 °C), CaB_6 nanowires with a tapered shape were observed as illustrated in Figures 4c,d. Catalytic particles were found at the tips of the nanowires. At even higher temperature (880−900 °C), CaB_6 nanowires with relatively uniform diameter were synthesized. Catalytic particles with different size and shape were observed. For example, Figure 4f shows a round-shaped particle, and Figure 4h shows a bullet-shaped particle.

To explore the growth mechanism(s) of these CaB_6 nanowires, a series of experiments were carried out. First, pyrolysis of B_2H_6 directly over CaO powder without introducing any Ni yielded no CaB_6 nanowires. Second, in addition to Ni, catalytic materials such as gold (Au) and platinum/palladium (Pt/Pd: 80/20) alloy were employed during synthesis. It was found that the Pt/Pd alloy could also catalyze the growth of CaB_6 nanowires. Third, different substrate materials (sapphire and single-crystal quartz) were used in addition to the typical Si wafer piece having a 1 μm

thick oxide layer. For each of these three substrates, the Ni-assisted growth of CaB_6 nanowires was observed by pyrolysis of B_2H_6 over CaO powders.

Given that (i) the CaB_6 nanowires grew only in the presence of certain metal catalysts, (ii) catalytic particles were observed on the tip of most nanowires, and (iii) the reaction temperature (860−900 °C) was lower than most reported values for synthesis of CaB_6 powders (>1000 °C), the growth of CaB_6 nanowires is probably due to the vapor−liquid−solid (VLS) mechanism.[42] Three possible main steps involved in the VLS growth are outlined as follows.

1. Generation of vapor phases. At elevated temperature, the pyrolysis of B_2H_6 produces a variety of gas-phase products, such as boron, hydrogen, borane radicals (e.g., $^{\bullet}BH_3$, $^{\bullet}BH_2$), and other higher boranes (e.g., B_4H_{10}, B_5H_{11}, $B_{10}H_{14}$, and others).[43] The vaporization of CaO also generates a range of gaseous species. Those detected by high-temperature mass spectrometry include (i) Ca(g), O_2(g), O(g) and CaO(g) produced by dissociation and sublimation of CaO,[44,45] and (ii) Ca(g), H_2(g), CaOH(g), and $Ca(OH)_2$(g) produced by heating of CaO in a H_2 environment.[46] We note that, according to the literature, the vapor pressure of the above Ca-containing gaseous species is low ($\sim 10^{-14}$ Torr) at the reaction temperature we used (~900 °C).[45−47] It has been reported that vaporization of Al_2O_3 at 760 Torr was observed at 2020 °C, whereas vaporization of Al_2O_3 at 3−8 Torr was observed at only 1690 °C.[48] Accordingly, we hypothesize that in the highly reducing chemical environment and low-pressure conditions of our reaction chamber, vapor species arising from CaO may be present at the relatively low temperatures used (~900 °C), via localized vaporization. Thus, gas-phase molecules and atomic and molecular free radicals including those produced from CaO through reaction with various gas-phase species, and those produced by pyrolysis of B_2H_6, may coexist in this environment.

2. Formation of liquid droplet. At elevated temperature, it is likely that the thin Ni film breaks up into small Ni particles available to react with the various Ca- and B-containing gaseous species discussed above. Although detailed information on the ternary phase diagram of Ca−B−Ni is not available,[49] small miscible Ca−B−Ni liquid alloy droplets may be formed and act as nucleation sites in the VLS growth of CaB_6 nanowires. As pointed out in Figure 2e and above, Si was also detected in the catalytic particles. We suggest that the presence of Si might lower the eutectic temperature of the liquid droplet (e.g., B−Ni, 1018 °C;[50] B−Ni−Si, 990 °C[49]). Deliberate addition of Si has been used to assist formation of molten Au/Si/B catalyst droplets for B nanowire synthesis.[34] In our reaction chamber, the sources of Si may include (i) impurity from CaO (the certificate provided by Alfa Aesar quoted 1−3 ppm Si for the high purity CaO powder), or (ii) Si from the substrate and quartz tube used.

3. Growth of nanowires. From the discussion above, one may speculate that a continuous supply of gas-phase Ca- and B-containing molecules cause the liquid Ca/B/Ni/Si droplets to become supersaturated, resulting in the precipitation of CaB_6 as nanowires by the VLS growth mechanism. Because of the presence of O_2 and O in the gas phase, the periphery of CaB_6 nanowires were oxidized, forming an amorphous calcium borate layer.

In addition to the possible VLS growth mechanism, vapor−solid (VS) growth of CaB_6 nanowires may coexist in the reaction chamber. We suggest that the combination of VLS and VS growth is responsible for the growth of tapered CaB_6 nanowires (Figure 4a−d) at lower temperature. The continuous growth of CaB_6 nanowires along the longitudinal direction is achieved via the VLS mechanism (as discussed above), whereas lateral growth is typically realized via the VS mechanism ($Ca + 6B \rightarrow CaB_6$, which could occur without catalyst[21]). In this scenario, the bottom portion of CaB_6 nanowires formed at the earlier stages develops a larger diameter due to both the VLS and VS growth, resulting in the tapered structure observed by SEM/TEM.

In our LPCVD system, pyrolysis of B_2H_6 (for the center temperature of 900 °C used here) occurs extensively near the inlet of the reaction chamber. Thus, additional B-containing gaseous species are available in the inlet region, including for the lower temperature range region depicted in Figure 4a,b. These B-containing species could solidify via the VS mechanism ($B(g) \rightarrow B(s)$). The B species are likely to deposit on the CaO powder, thus preventing localized vaporization of CaO. This prevents CaB_6 nanowire growth by either the VLS or VS mechanism, while at the same time producing a B-containing amorphous shell surrounding the nanowire. The result is the formation of short nanowires with a thick amorphous B-containing shell (Figure 4a,b).

To test our hypothesis for the mechanism(s) of growth of the CaB_6 nanowires suggested above, knowledge of the spatial distribution of the gas-phase species (reactants and products) in both the growth region and upstream and downstream of the growth region would be helpful. For example, in-line mass spectrometer sampling of the gas-phase species is a capability we hope to add in the future to our home-built LPCVD system.

In summary, catalyst-assisted growth of single-crystal CaB_6 nanowires by pyrolysis of B_2H_6(g) over CaO(s) powder at 860−900 °C and ~155 mTorr was achieved using a home-built LPCVD system; Ni and Pt/Pd are effective catalysts. The nanowires have diameters of ~15−40 nm and lengths of ~1−10 μm. Growth is probably by the VLS mechanism. This synthesis of single-crystal CaB_6 nanowires opens the possibility of study of their physical and chemical properties.

Acknowledgment. We appreciate the support of the National Science Foundation (R.S.R.: grant EEC-0210120), and the Office of Naval Research grant (R.S.R.: No. N000140210870; program manager: Mark Spector). We are grateful to the NUANCE facility at Northwestern University for SEM and TEM measurements, and the RRC facility at the University of Illinois-Chicago for TEM and Raman spectra measurements. The authors appreciate comments by K. Kohlhaas and D. Cantrell.

References

(1) *Boron, Metallo-Boron, Compounds and Boranes*; Adams, R. M., Ed.; Interscience Publishers: New York, 1964; p 233.
(2) *Boron and Refractory Borides*; Matkovich, V. I., Ed.; Springer-Verlag: Berlin, 1977.
(3) Takeda, M.; Fukuda, T.; Domingo, F.; Miura, T. *J. Solid State Chem.* **2004**, *177*, 471.
(4) Imai, Y.; Mukaida, M.; Ueda, M.; Watanabe, A. *Intermetallics* **2001**, *9*, 721.
(5) Young, D. P.; Hall, D.; Torelli, M. E.; Fisk, Z.; Sarrao, J. L.; Thompson, J. D.; Ott, H. R.; Oseroff, S. B.; Goodrich, R. G.; Zysler, R. *Nature* **1999**, *397*, 412.
(6) Otani, S.; Mori, T. *J. Phys. Soc. Jpn.* **2002**, *71*, 1791.
(7) Akimitsu, J.; Takenawa, K.; Suzuki, K.; Harima, H.; Kuramoto, Y. *Science* **2001**, *293*, 1125.
(8) Zhitomirsky, M. E.; Rice, T. M.; Anisimov, V. I. *Nature* **1999**, *402*, 251.
(9) Murakami, S.; Shindou, R.; Nagaosa, N.; Mishchenko, A. S. *J. Phys. Chem. Solids* **2002**, *63*, 1285.
(10) Matsubayashi, K.; Maki, M.; Tsuzuki, T.; Nishioka, T.; Sato, N. K. *Nature* **2002**, *420*, 143.
(11) Mori, T.; Otani, S. *Solid State Commun.* **2002**, *123*, 287.
(12) Bennett, M. C.; van Lierop, J.; Berkeley, E. M.; Mansfield, J. F.; Henderson, C.; Aronson, M. C.; Young, D. P.; Bianchi, A.; Fisk, Z.; Balakirev, F.; Lacerda, A. *Phys. Rev. B* **2004**, *69*.
(13) Kino, H.; Aryasetiawan, F.; van Schilfgaarde, M.; Kotani, T.; Miyake, T.; Terakura, K. *J. Phys. Chem. Solids* **2002**, *63*, 1595.
(14) Hasegawa, A.; Yanase, A. *J. Phys. C − Solid State Phys.* **1979**, *12*, 5431.
(15) Massidda, S.; Continenza, A.; dePascale, T. M.; Monnier, R. *Z. Phys. B: Condens. Matter* **1997**, *102*, 83.
(16) Tromp, H. J.; van Gelderen, P.; Kelly, P. J.; Brocks, G.; Bobbert, P. A. *Phys. Rev. Lett.* **2001**, *8701*.
(17) Souma, S.; Komatsu, H.; Takahashi, T.; Kaji, R.; Sasaki, T.; Yokoo, Y.; Akimitsu, J. *Phys. Rev. Lett.* **2003**, *90*.
(18) Dutta, S. K. *Am. Ceram. Soc. Bull.* **1975**, *54*, 727.
(19) Otani, S. *J. Cryst. Growth* **1998**, *192*, 346.
(20) Otani, S.; Mori, T. *J. Mater. Sci. Lett.* **2003**, *22*, 1065.
(21) Johnson, R. W.; Danne, A. H. *J. Chem. Phys.* **1963**, *38*, 425.
(22) Zheng, S. Q.; Min, G. H.; Zou, Z. D.; Yu, H. S.; Han, H. D. *J. Am. Ceram. Soc.* **2001**, *84*, 2725.
(23) Shi, L.; Gu, Y. L.; Chen, L. Y.; Yang, Z. C.; Ma, J. H.; Qian, Y. T. *Chem. Lett.* **2003**, *32*, 958.
(24) Boustani, I.; Quandt, A.; Hernandez, E.; Rubio, A. *J. Chem. Phys.* **1999**, *110*, 3176.
(25) Quandt, A.; Liu, A. Y.; Boustani, I. *Phys. Rev. B* **2001**, *6412*.
(26) Cao, L. M.; Zhang, Z.; Sun, L. L.; Gao, C. X.; He, M.; Wang, Y. Q.; Li, Y. C.; Zhang, X. Y.; Li, G.; Zhang, J.; Wang, W. K. *Adv. Mater.* **2001**, *13*, 1701.
(27) Zhang, Y. J.; Ago, H.; Yumura, M.; Komatsu, T.; Ohshima, S.; Uchida, K.; Iijima, S. *Chem. Commun.* **2002**, *23*, 2806.
(28) Otten, C. J.; Lourie, O. R.; Yu, M. F.; Cowley, J. M.; Dyer, M. J.; Ruoff, R. S.; Buhro, W. E. *J. Am. Chem. Soc.* **2002**, *124*, 4564.
(29) Yang, Q.; Sha, J.; Xu, J.; Ji, Y. J.; Ma, X. Y.; Niu, J. J.; Hua, H. Q.; Yang, D. R. *Chem. Phys. Lett.* **2003**, *379*, 87.
(30) Meng, X. M.; Hu, J. Q.; Jiang, Y.; Lee, C. S.; Lee, S. T. *Chem. Phys. Lett.* **2003**, *370*, 825.
(31) Wang, Z. K.; Shimizu, Y.; Sasaki, T.; Kawaguchi, K.; Kimura, K.; Koshizaki, N. *Chem. Phys. Lett.* **2003**, *368*, 663.
(32) Xu, T. T.; Zheng, J. G.; Wu, N. Q.; Nicholls, A. W.; Roth, J. R.; Dikin, D. A.; Ruoff, R. S. *Nano Lett.* **2004**, *4*, 963.
(33) Ma, J. H.; Gu, Y. L.; Shi, L.; Chen, L. Y.; Yang, Z. H.; Qian, Y. T. *Chem. Phys. Lett.* **2003**, *381*, 194.
(34) Wu, Y. Y.; Messer, B.; Yang, P. D. *Adv. Mater.* **2001**, *13*, 1487.
(35) Ma, R. Z.; Bando, Y.; Mori, T.; Golberg, D. *Chem. Mater.* **2003**, *15*, 3194.
(36) Ogita, N.; Nagai, S.; Okamoto, N.; Iga, F.; Kunii, S.; Akimitsu, J.; Udagawa, M. *Phys. Rev. B: Condens. Matter* **2003**, *328*, 131.
(37) Yahia, Z.; Turrell, S.; Mercurio, J. P.; Turrell, G. *J. Raman Spectrosc.* **1993**, *24*, 207.
(38) Richter, H.; Wang, Z. P.; Ley, L. *Solid State Commun.* **1981**, *39*, 625.
(39) Campbell, I. H.; Fauchet, P. M. *Solid State Commun.* **1986**, *58*, 739.
(40) Piscanec, S.; Cantoro, M.; Ferrari, A. C.; Zapien, J. A.; Lifshitz, Y.; Lee, S. T.; Hofmann, S.; Robertson, J. *Phys. Rev. B* **2003**, *68*, 241312.
(41) Yahia, Z.; Turrell, S.; Turrell, G. *J. Mol. Struct.* **1990**, *224*, 303.
(42) Wagner, R. S.; Ellis, W. C. *Trans. Metall. Soc. AIME* **1965**, *233*, 1053.
(43) Greenwood, N. N.; Earnshaw, A. *Chemistry of the Elements*; Reed Educational and Professional Publishing Ltd: UK, 1997; p 139.
(44) Samoilova, I. O.; Kazenas, E. K. *Metally* **1995**, *1*, 33.
(45) Farber, M.; Srivastava, R. D. *High Temp. Sci.* **1976**, *8*, 73.
(46) Farber, M.; Srivastava, R. D.; Moyer, J. W.; Leeper, J. D. *J. Chem. Soc., Faraday Trans.* **1987**, *83*, 3229.
(47) *The Oxide Handbook*; Samsonov, G. V., Ed.; IFI/Plenum: New York, 1973.
(48) Otto, R. *Angew. Chem.* **1912**, *24*, 1459.
(49) Villars, P.; Prince, A.; Okamoto, H. *Handbook of Ternary Alloy Phase Diagrams*; ASM International: Materials Park, OH, 1995.
(50) Okamoto, H. *Desk Handbook: Phase Diagrams for Binary Alloys*; ASM International: Materials Park, OH, 2000.

NL0486620